



Amidoxime covalent organic framework@Fe₃O₄ based magnetic solid-phase extraction for rapid and sensitive determination of trace uranium in seafood

Fan Bai^b, Xu Yang^b, Cheng Yang^b, Hai-Long Qian^{a,b,*}, Xiu-Ping Yan^{a,b,c}

^a State Key Laboratory of Food Science and Resource, Jiangnan University, Wuxi 214122, China

^b Institute of Analytical Food Safety, School of Food Science and Technology, Jiangnan University, Wuxi 214122, China

^c Key Laboratory of Synthetic and Biological Colloids, Ministry of Education, Jiangnan University, Wuxi 214122, China

ARTICLE INFO

Keywords:

Uranium

MSPE

Amidoxime functionalized COF

ABSTRACT

The unintentional dissemination of uranium into environment poses substantial risks to both food sources and human populations. An advanced method for convenient and accurate detection of uranium in food is thus a pressing need. Herein, a novel magnetic amidoxime functionalized covalent organic framework (TpDb-AO@Fe₃O₄), prepared with 2,5-dinitrobenzonitrile, 1,3,5-triformylphloroglucinol and hydroxylamine hydrochloride, was synthesized as adsorbent for magnetic-solid phase extraction (MSPE) of UO₂²⁺. Furthermore, a TpDb-AO@Fe₃O₄ based MSPE coupled with UV-vis spectrophotometer was successfully developed to realize the determination of uranyl ions with low limit of detection of 1.63 μg L⁻¹, wide linear range of 10 – 200 μg L⁻¹. The spiking recoveries in real seafood samples (tuna, yesso scallop, kelp, eel, hairtail) ranged from 94.1 % – 106.8 %. The intraday (*n* = 5) and interday (*n* = 5) relative standard deviation (RSD) for determination of UO₂²⁺ were 3.33 % and 6.23 %, respectively. This approach represents an advancement in the rapid extraction and sensitive quantification of trace uranium contaminants in food matrices, thereby contributing to enhanced environmental monitoring and public health safeguards.

1. Introduction

Nuclear power generation as clean energy will play an important role in addressing energy shortages and greenhouse effect over the next 100 years [1]. However, nuclear accidents and inadequate management of nuclear waste would result in the migration of radioactive contaminants throughout ecosystems and food chains [2,3]. Of particular concern is uranium, which predominantly exists as soluble uranyl ions, readily infiltrating water bodies and accumulating in aquatic life, such as bivalves and fish, as well as vegetation [4,5]. The long-term exposure can lead to a series of severe health hazards, such as damage to the kidneys, bones, liver, reproduction, urinary, DNA [6–9]. The World Health Organization has already set a stringent limit of 30 μg L⁻¹ for uranium in its 2022 Guidelines for drinking-water quality [10]. Therefore, the precise detection of trace uranium is of great significance to safeguard both environmental integrity and public health.

The low concentration of uranium and severe matrix interference in real samples make it necessary to enrich uranium prior to instrumental

analysis. Magnetic-solid phase extraction (MSPE) is generally acknowledged as a simple, efficient, and eco-friendly technology owing to its magnetic separation property [11–13], and thereby is the preferred candidate for sample pretreatment of uranium in complex samples. Various functional materials, including ion-imprinted polymers [14,15], carbon nanotubes [16], metal organic framework (MOF) [17,18] and graphene oxide [17,19] have been composited with magnetic nanoparticles (NPs) to engineer highly advanced magnetic adsorbent for the detection of uranium, but these materials always suffer from the sluggish adsorption rates or insufficient stability in complex matrix.

Covalent organic frameworks (COFs) have drawn growing interest in sample preparation due to their high surface area, ordered pore channels, adjustable pore size, and good stability. COFs have already been used as adsorbents for removal of uranium. Qiu et al. first introduced the amidoxime groups into COFs for adsorption of uranium. The amidoxime can coordinate with uranium in both monodentate and tridentate manners, making it a state-of-the-art group for adsorption of uranium [20]. Since then, diverse amidoxime and its derivatives functionalized

* Corresponding authors.

E-mail address: hlqian@jiangnan.edu.cn (H.-L. Qian).

<https://doi.org/10.1016/j.chroma.2024.465564>

Received 9 October 2024; Received in revised form 22 November 2024; Accepted 27 November 2024

Available online 28 November 2024

0021-9673/© 2024 Elsevier B.V. All rights reserved, including those for text and data mining, AI training, and similar technologies.

COFs have been reported for highly selective adsorption and removal of uranium [21–25]. These studies lay the foundation for amidoxime COFs as an alternative solution for the selective extraction of trace uranium and the development of efficient detection methods for trace uranium in complex samples, but the related investigations in this area have been rarely reported so far.

Herein, we present the synthesis of a novel magnetic adsorbent, comprised of an amidoxime COF integrated with Fe_3O_4 NPs, and development of MSPE based analytical method for rapid and sensitive determination of trace uranium. Amidoxime functionalities have been well-established for the high selectivity towards uranium due to the specific chelation capability of amidoxime with uranium species [25–27]. Accordingly, an amidoxime COF of TpDb-AO, prepared with 2,5-dinitrobenzonitrile (Db), 1,3,5-triformylphloroglucinol (Tp) and hydroxylamine hydrochloride ($\text{NH}_2\text{OH}\cdot\text{HCl}$), was designed to compose with Fe_3O_4 via amorphous-to-crystalline transformation to obtain magnetic COF (TpDb-AO@ Fe_3O_4). Then the TpDb-AO@ Fe_3O_4 based MSPE was developed to couple with UV–vis spectrophotometer, enabling the efficient determination of uranyl ions in complex, real seafood samples.

2. Chemicals and materials

2.1. Chemical reagents

Tp and Db were obtained from CHEMSOON Chemical Technology Co., Ltd. (Shanghai, China). Uranyl nitrate hexahydrate, trimethylamine, $\text{NH}_2\text{OH}\cdot\text{HCl}$, 1,3,5-trimethylbenzene, 1,2-dichlorobenzene, arsenazo III and ferric chloride hexahydrate ($\text{FeCl}_3\cdot 6\text{H}_2\text{O}$) were all purchased from Aladdin Biochemical Technology Co., Ltd. (Shanghai, China). Perchloric acid, NaOH, KBr, H_2O_2 (30 %), Na_2CO_3 , HCl, HNO_3 , methanol, tetrahydrofuran (THF), ethanol, CH_3COONa , 1,6-diaminohexane, ethylene glycol (EG), acetic acid (HAc), 1,4-dioxane and n-Butanol were sourced from Sinopharm Chemical Reagent Co., Ltd. (Shanghai, China). Ultrapure water was from Wahaha Foods Co. Ltd (Hangzhou, China). Aqueous filtration membrane (0.22 μm) was bought from Agilent Technology Co., Ltd. (Suzhou, China). The uranium stock solution is 1 g L^{-1} of uranyl nitrate hexahydrate. The working solution was derived through sequential diluting the uranium stock solution by a nitric acid solution with a pH of 6.

2.2. Synthesis of the Fe_3O_4 and TpDb-AO@ Fe_3O_4

Magnetic Fe_3O_4 NPs were prepared according to a previously reported protocol [28]. In short, 2.0 g $\text{FeCl}_3\cdot 6\text{H}_2\text{O}$ was ultrasonically dispersed in 60 mL of EG for 10 min, then 10 mL 1,6-hexadiazine and 6.0 g CH_3COONa were added to the mixture, which was then stirred at 50 °C until homogeneity. The mixture was finally heated at 200 °C for 8 h, and the product was washed thrice with ultrapure water and ethanol and dried in a vacuum oven at 60 °C for 6 h to obtain Fe_3O_4 NPs.

The TpDb-AO@ Fe_3O_4 was prepared via the amorphous-to-crystalline conversion [28,29]. Fe_3O_4 NPs (28 mg) was mixed with Tp (21 mg) in THF (7 mL) and 6 mol L^{-1} HAc (1.2 mL) under ultrasonication for 10 min, heated at 50 °C for 2 h, then Db (19.9 mg) dissolved in 5 mL THF was added under ultrasonication for another 5 min, and heating was continued for an additional 6 h at the same temperature. The product was collected using magnetic separation. After repeating the above process for 3 times, a polymer@ Fe_3O_4 was obtained. Next, 150 mg polymer@ Fe_3O_4 was dispersed in 2.2 mL mixture of 1,4-dioxane, mesitylene and 6 mol L^{-1} HAc (5:5:1, v:v:v), sonicated for 5 min, degassed with three freeze-pump-thaw cycles, heated at 120 °C for 5 d, Soxhlet extracted with THF for 1 d, and dried in a vacuum oven at 60 °C for 6 h to obtain TpDb-CN@ Fe_3O_4 . Finally, the TpDb-CN@ Fe_3O_4 (200 mg), $\text{NH}_2\text{OH}\cdot\text{HCl}$ (400 mg) and trimethylamine (1 mL) were mixed in 5 mL methanol under ultrasonication for 10 min, degassed by three freeze-pump-thaw cycles, and heated at 70 °C for 2 h. The resulting

product was washed with water and freeze-dried to yield the targeted TpDb-AO@ Fe_3O_4 .

2.3. Sample preparation

Real tuna, eel, hairtail, yesso scallops and kelp samples were bought from the local market. Typically, the edible parts of the samples were cleaned with ultrapure water, then dried with a towel and chopped into smaller pieces using scissors. The 40 g chopped sample was put into a round-bottom glass digestion tube, followed by the addition of 30 mL HNO_3 for cold digestion over a period of 10 h. Subsequently, 6 mL H_2O_2 (30 %) was added for further digestion at 120 °C for another 4 h, and then acid was evaporated nearly to dryness using a graphite digestion system at 100 °C. The residue was then reconstituted with aqueous solution (pH 6) to a fixed volume of 40 mL. The spiked samples were obtained by adding different concentrations of UO_2^{2+} into original samples before digestion.

2.4. MSPE procedure

10 mg TpDb-AO@ Fe_3O_4 was added into 40 mL of sample solution, and agitated on an oscillator for 50 min, and discarded from the aqueous phase by a magnetic separation. Subsequently, the adsorbent was washed with 1.2 mol L^{-1} HCl (1.5 mL) for 20 min and the eluate was collected and filtered through a 0.22 μm aqueous filtration membrane, dried in nitrogen at 65 °C, the residue was redissolved with 0.4 mL HCl (1.2 mol L^{-1}) for further detection of UO_2^{2+} .

2.5. Detection of UO_2^{2+}

UO_2^{2+} can form a complex with chromogenic agent of arsenazo III (UO_2^{2+} -arsenazo-III), which gave a characterized UV–vis absorption peak at 651 nm [30]. Accordingly, 0.4 mL arsenazo III was first mixed with 0.4 mL sample, and after a brief 5-minute agitation, the UV-visible absorbance spectrum (with a slit width of 1 nm) was recorded across a wavelength range of 620 to 700 nm. The absorbance intensity at 651 nm was taken for the quantification of uranium.

3. Results and discussion

3.1. Preparation of TpDb-AO@ Fe_3O_4

Since COF typically need to be synthesized at high temperature and pressure, which pose challenges to the conventional in-situ growth methodology for composite fabrication, an alternative amorphous-to-crystalline transformation strategy has been devised to address this limitation [28]. Accordingly, the Tp and Db were first in-situ grown with Fe_3O_4 NPs at mild and atmospheric conditions to form an amorphous polymer-coated Fe_3O_4 (polymer@ Fe_3O_4), then this amorphous polymer is converted into crystalline cyanide COF at high temperature and pressure to yield TpDb-CN@ Fe_3O_4 . Finally, the TpDb-CN is chemically modified to amidoxime COF with $\text{NH}_2\text{OH}\cdot\text{HCl}$ to prepared the targeted TpDb-AO@ Fe_3O_4 (Fig. 1).

The appearance of characterized powder X-ray diffraction (PXRD) peaks of TpDb-CN and TpDb-AO indicates the feasibility of preparing COF TpDb-AO via amorphous-to-crystalline approach (Fig. S1). 400 mg of $\text{NH}_2\text{OH}\cdot\text{HCl}$ led to the disappearance of stretching vibration fourier transform infrared (FTIR) peak for cyano group (Fig. S2), demonstrating the complete modification of cyano to amidoxime. Repeating the polymer growth cycle three and four times resulted in the appearance of PXRD peaks for TpDb-CN (Fig. S3). However, the saturation magnetization of the composite decreased from 18.6 emu g^{-1} to 12.6 emu g^{-1} when increasing the reaction cycles from three to four (Fig. S4), so a three-cycle polymerization process was chosen as the synthesis condition.

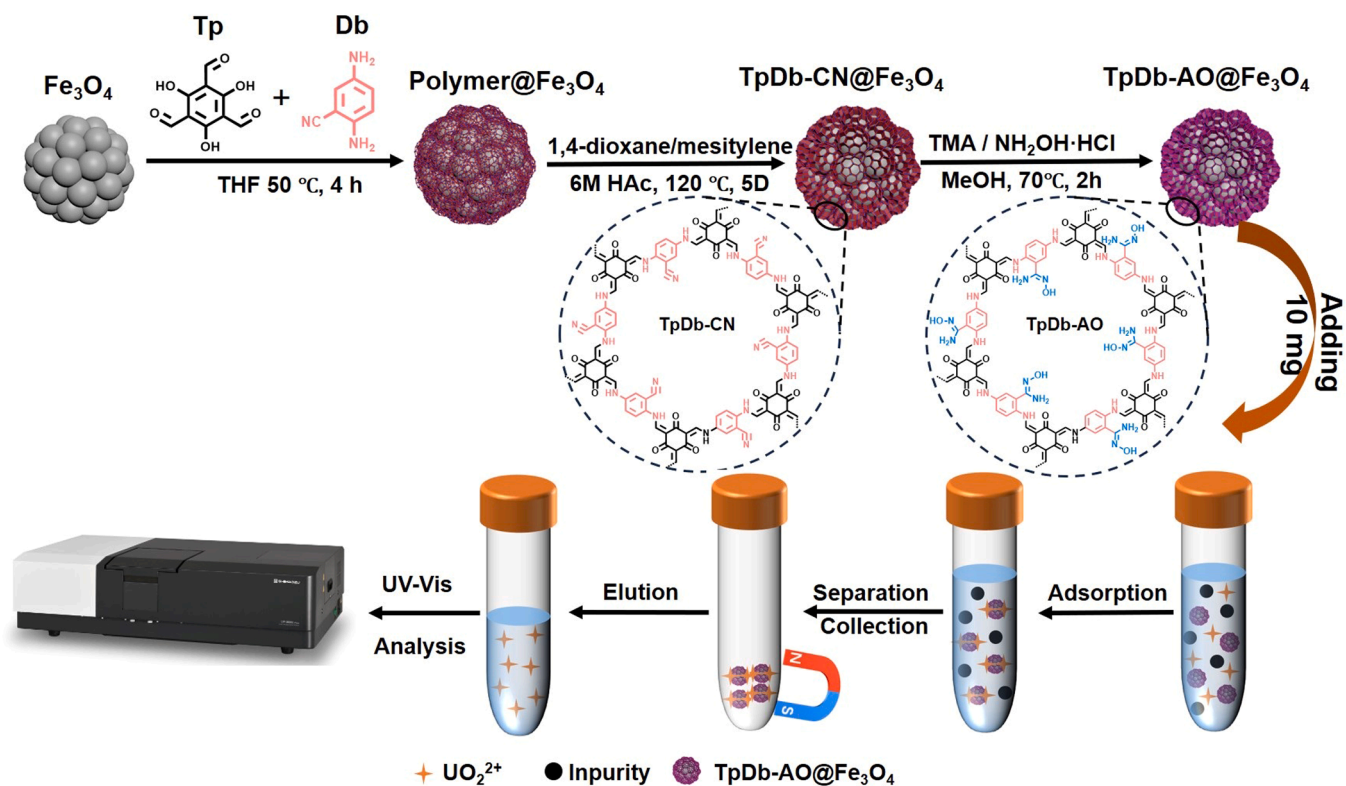


Fig. 1. Schematic diagram for preparation of TpDb-AO@Fe₃O₄ and magnetic solid phase extraction of UO₂²⁺.

3.2. Characterization of TpDb-AO@Fe₃O₄

The morphology of Fe₃O₄ NPs, TpDb-AO and TpDb-AO@Fe₃O₄ were observed by scanning electron microscope (SEM) and transmission electron microscope (TEM). As shown in Fig. 2a and d, Fe₃O₄ NPs exhibited spherical-like morphology. In contrast, the TpDb-AO was found to adopt a rod-like shape (Fig. 2b and e). The presence of discernible spherical Fe₃O₄ particles within the rod-shaped TpDb-AO matrix served as clear evidence of the successful preparation of TpDb-

AO@Fe₃O₄ composite (Fig. 2c and f).

Both TpDb-CN and TpDb-AO gave similar PXRD patterns, featuring a prominent peak at 4.7° (Fig. S5). The main peaks in PXRD pattern of Fe₃O₄ NPs at 30.1°, 35.5°, 43.1°, 56.9° and 62.5° proved valid crystal of the prepared Fe₃O₄ (Fig. S6). The prepared TpDb-AO@Fe₃O₄ gave the appearance of both main PXRD peaks of TpDb-AO and Fe₃O₄ (Fig. 3a). Furthermore, the existence of stretching vibration peak of Fe-O (590 cm⁻¹) and C-N (1278 cm⁻¹) coupled with the absence of cyano group peak at 2216 cm⁻¹ (Fig. 3b and S7), confirmed the successful growth of

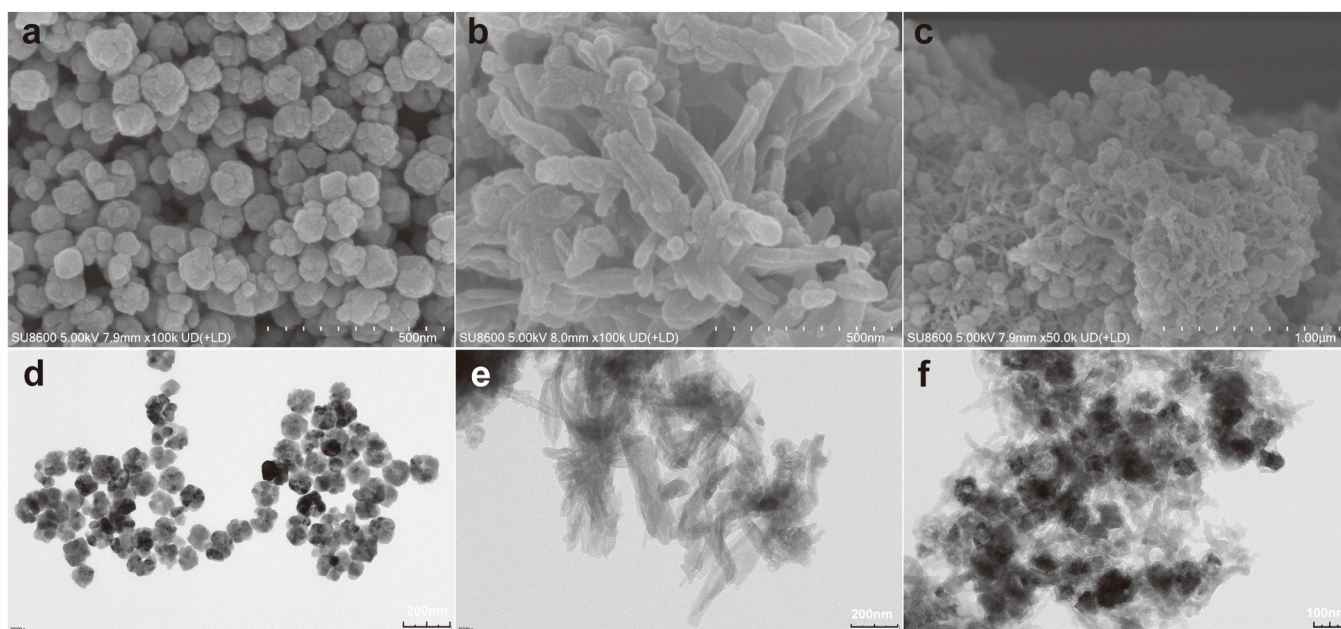


Fig. 2. SEM and TEM images of (a, d) Fe₃O₄, (b, e) TpDb-AO and (c, f) TpDb-AO@Fe₃O₄.

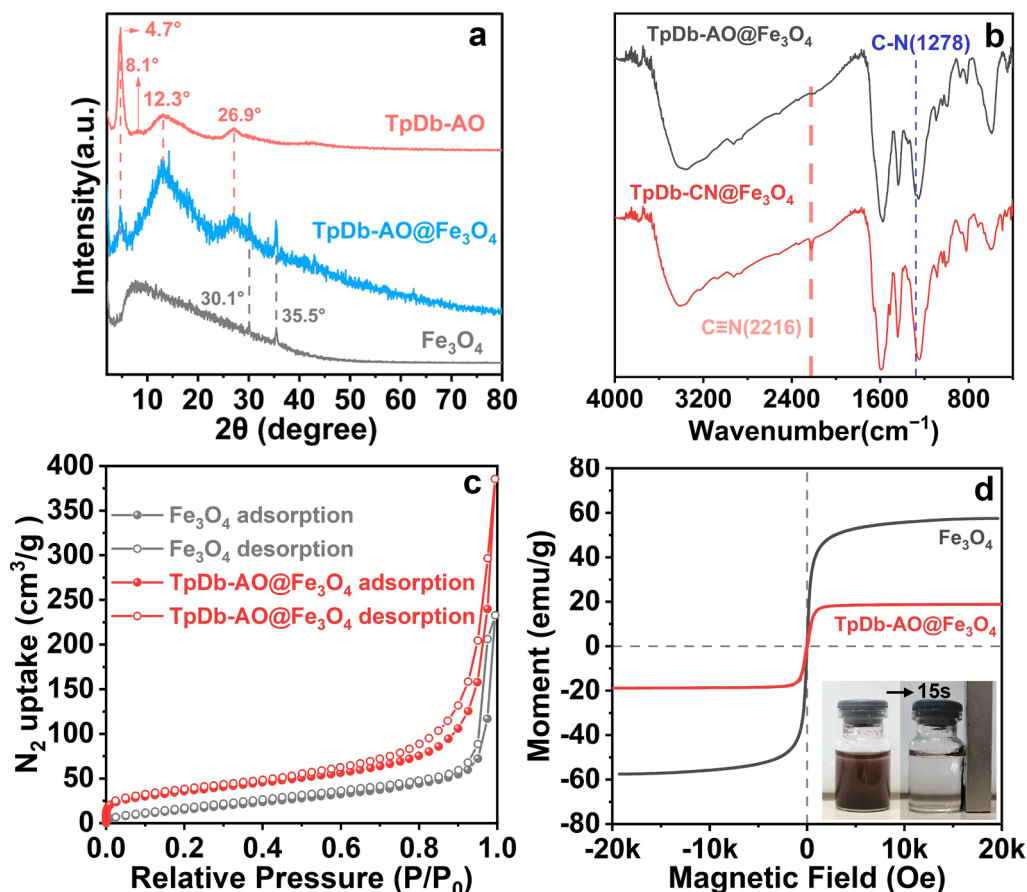


Fig. 3. (a) PXRD patterns of Fe₃O₄ NPs, TpDb-AO and TpDb-AO@Fe₃O₄; (b) FTIR spectra of TpDb-CN@Fe₃O₄ and TpDb-AO@Fe₃O₄; (c) N₂ adsorption–desorption isotherms of Fe₃O₄ and TpDb-AO@Fe₃O₄; (d) VSM characteristics of Fe₃O₄ NPs and TpDb-AO@Fe₃O₄.

TpDb-AO on the Fe₃O₄ NPs.

Compared with the Fe₃O₄ NPs (0.155 cm³ g⁻¹ and 72.0 m² g⁻¹), the TpDb-AO@Fe₃O₄ gave a higher pore volume of 0.327 cm³ g⁻¹ and BET surface area of 128.6 m² g⁻¹ (Fig. 3c), which would promote the adsorption ability for the target. The magnetic properties of Fe₃O₄ and TpDb-AO@Fe₃O₄ were studied by vibrating sample magnetometry (VSM) (Fig. 3d). Although the magnetic saturation value decreased from 57.5 emu g⁻¹ to 18.6 emu g⁻¹ after the introduction of non-magnetic COF TpDb-AO, the composite TpDb-AO@Fe₃O₄ can achieve magnetic separation in 15 s, which is sufficient for the magnetic solid-phase extraction. The retention of PXRD patterns of TpDb-AO@Fe₃O₄ after treatment in 2 mol L⁻¹ HCl, 2 mol L⁻¹ NaOH and 2 mol L⁻¹ NaCl for 24 h (Fig. S8), indicating the good stability of the prepared magnetic composite.

3.3. Adsorption performance of TpDb-AO@Fe₃O₄

The effect of time on the adsorption capacity of TpDb-AO@Fe₃O₄ for UO₂²⁺ confirmed the adsorption equilibrium time is approximately 50 min (Fig. 4a). The adsorption capacity can quickly reach to exceed 60 % of the equilibrium adsorption capacity in 5 min, due to the large concentration gradient and abundant active sites at the beginning of adsorption. Then adsorption capacity increased slowly, because of the slow interaction between UO₂²⁺ and the interfering substances occupied sites. The corresponding adsorption kinetics adopt to the quasi-second-order kinetic model rather than quasi-first-order kinetic model (Fig. 4b and c). Furthermore, the adsorption of UO₂²⁺ on TpDb-AO@Fe₃O₄ can be better described by Langmuir model than Freundlich model (Fig. 4d). Although the maximum adsorption capacity of TpDb-AO@Fe₃O₄ for UO₂²⁺ calculated from Langmuir model was 31.6 mg g⁻¹ mainly due to

the limited amount of TpDb-AO in the composite, it is sufficient for the extraction of trace UO₂²⁺. In the presence of high concentrations of different ions (K⁺, Mg²⁺, Na⁺, Ba²⁺, Ni²⁺, Ca²⁺, Zn²⁺, Fe³⁺ and Al³⁺), the K_d of TpDb-AO@Fe₃O₄ for UO₂²⁺ was significantly higher than for other ions, indicating the great selectivity of TpDb-AO@Fe₃O₄ for UO₂²⁺ (Fig.S9).

3.4. Optimization of MSPE

The amidoxime-functionalized COF and magnetic Fe₃O₄ NPs render the TpDb-AO@Fe₃O₄ magnetic selective adsorption to UO₂²⁺. Thereby, the TpDb-AO@Fe₃O₄ based MSPE was developed to extract the trace UO₂²⁺. The absorption intensity of UO₂²⁺–arsenazo-III complex at 651 nm (I₆₅₁) showed no significant alteration after 50 min, suggesting the completion of extraction within this timeframe (Fig. 5a). The I₆₅₁ enhanced with the increase of pH until pH 6. Further increase of pH led to decline of I₆₅₁, establishing pH 6 as the optimal condition for efficiency (Fig. 5b). 10 mg TpDb-AO@Fe₃O₄ was chosen for the extraction as increasing the adsorbent dosage beyond this point did not yield a substantial rise in I₆₅₁ (Fig. 5c). Similarly, the elution conditions of eluent, desorption time, eluent volume were investigated via monitoring the I₆₅₁. The results showed the UO₂²⁺ can be completely desorbed with elution of 1.5 mL 1.2 mol L⁻¹ HCl for 20 min (Fig. 5d–5f). The Fe ion in extracted solution and eluent was determined to be 0.7 μg L⁻¹ and 1.5 mg L⁻¹, respectively. The higher concentration of Fe in eluent may result from the slight decomposition of Fe₃O₄ by the HCl. The low residual Fe ion gave no evident effect on the I₆₅₁, indicating the negligible interference of residual Fe ion for the detection of UO₂²⁺ (Fig. S10).

The enhancement factor (EF) stands as a pivotal measure of extraction efficiency. According to the equation (SI), the EFs for UO₂²⁺ at

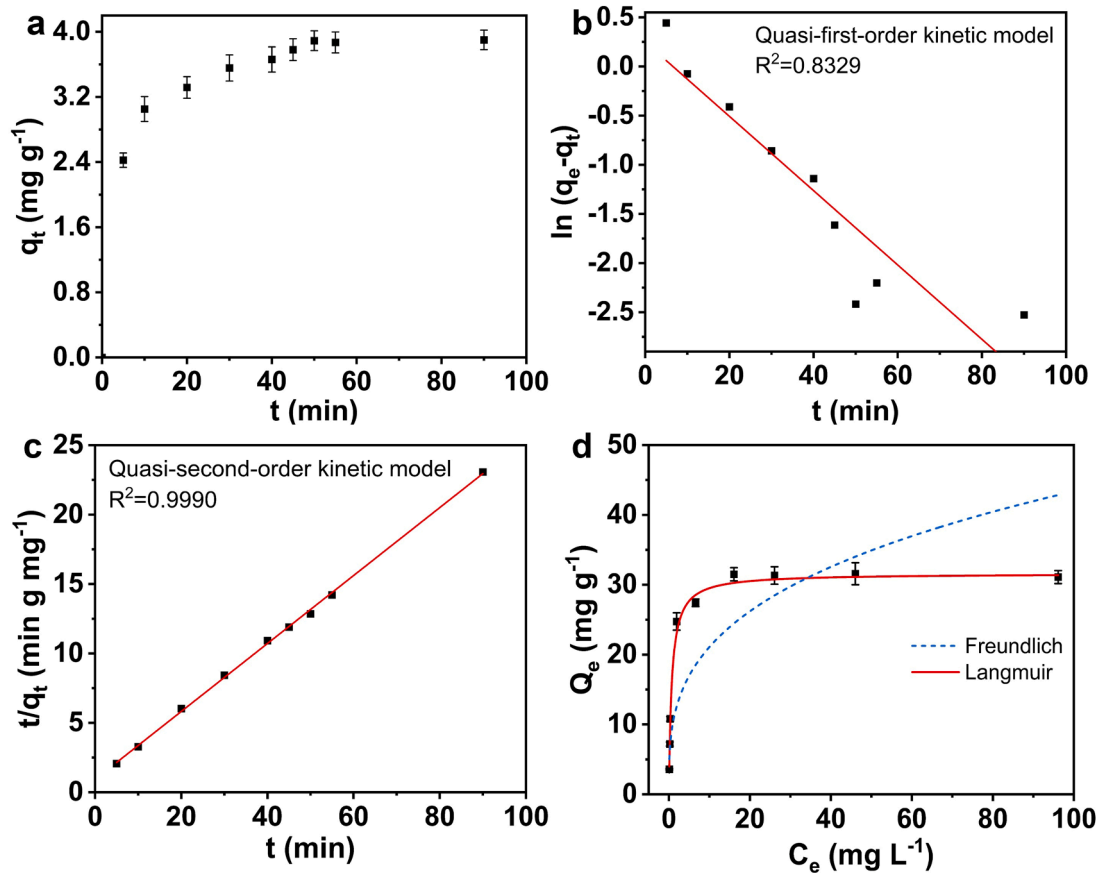


Fig. 4. (a) Effect of time on adsorption of UO_2^{2+} on $\text{TpDb-AO@Fe}_3\text{O}_4$. Fitting results of adsorption kinetics with (b) quasi-first-order kinetic model and (c) quasi-second-order kinetic model. (d) Fitting results of adsorption isotherms with Langmuir model and Freundlich model.

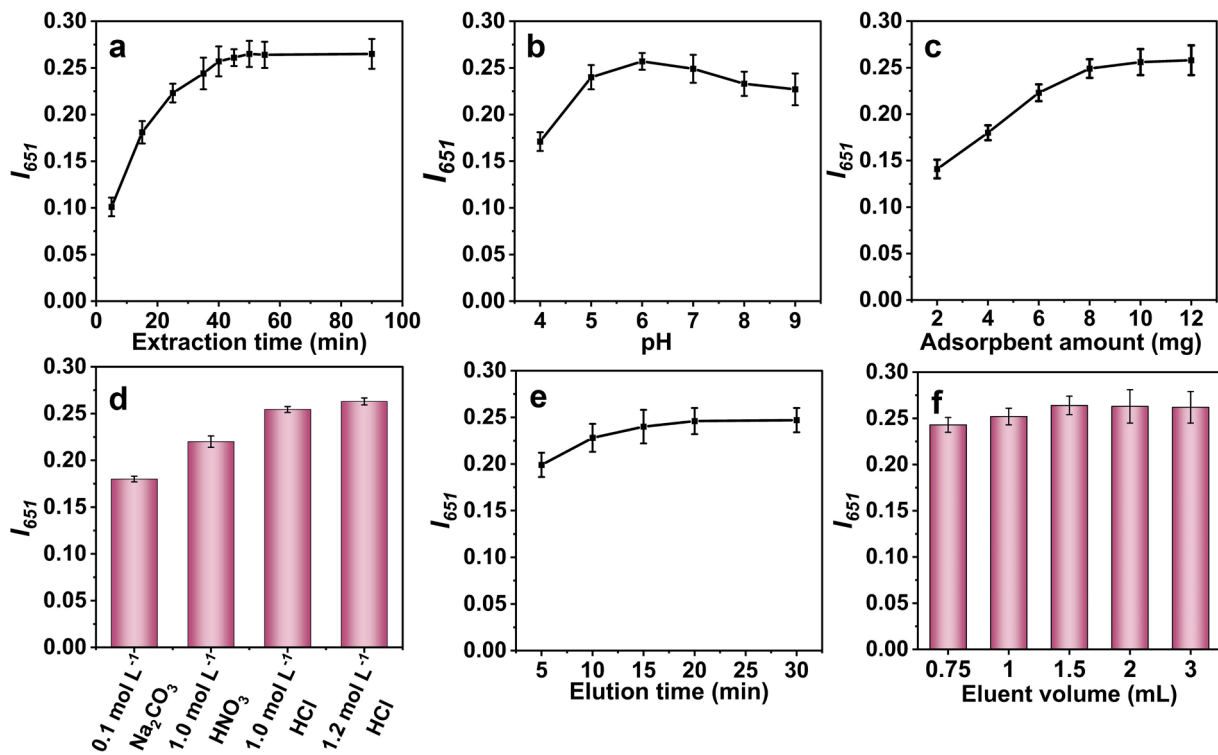


Fig. 5. Effect of (a) extraction time, (b) pH, (c) amount of $\text{TpDb-AO@Fe}_3\text{O}_4$, (d) type of eluent, (e) elution time, and (f) eluent volume on the I_{651} (The initial concentration of UO_2^{2+} was $50 \mu\text{g L}^{-1}$).

concentration of $50 \mu\text{g L}^{-1}$, $100 \mu\text{g L}^{-1}$ and $150 \mu\text{g L}^{-1}$ were 84.6, 82.3 and 81.2, respectively (Table S1). The I_{651} for UO_2^{2+} ($50 \mu\text{g L}^{-1}$) gave negligible reduction after six consecutive extraction cycles (Fig. S11). The FTIR and PXRD of $\text{TpDb-AO@Fe}_3\text{O}_4$ gave no obvious change after extraction compared with the original composite (Fig. S12 and S13), further highlighting the great reusability of the prepared $\text{TpDb-AO@Fe}_3\text{O}_4$.

The antisymmetric vibration of $[\text{O} = \text{U} = \text{O}]^{2+}$ in the FTIR of the composite spectra significantly shifted from 962 cm^{-1} to 939 cm^{-1} after the adsorption of UO_2^{2+} with $\text{TpDb-AO@Fe}_3\text{O}_4$ (Fig. S14), demonstrating the strong chemical coordination between the amidoxime group on $\text{TpDb-AO@Fe}_3\text{O}_4$ and UO_2^{2+} [31]. The zeta potential of $\text{TpDb-AO@Fe}_3\text{O}_4$ became more negative with the increase of pH (Fig. S15), while the uranium exists as cationic form at $\text{pH} < 6.5$ [32], indicating the involvement of electrostatic interaction in the adsorption. The rich coordination sites on $\text{TpDb-AO@Fe}_3\text{O}_4$ make it emerge as a promising candidate for the extraction of uranium from complex real samples.

3.5. Analytical figures of merit

The $\text{TpDb-AO@Fe}_3\text{O}_4$ based MSPE was further coupled with UV-vis to establish an analytical method for trace uranium. Assessing its analytical proficiency in standard solutions ranging from 1 to $1000 \mu\text{g L}^{-1}$, a robust linear correlation between concentration of UO_2^{2+} and I_{651} was attained in the range of $10\text{--}200 \mu\text{g L}^{-1}$ ($R^2 = 0.9986$) (Fig. S16). The developed $\text{TpDb-AO@Fe}_3\text{O}_4$ based MSPE-UV-vis exhibited a limit of detection (LOD) ($S/N = 3$) of $1.63 \mu\text{g L}^{-1}$ and limit of quantification (LOQ) ($S/N = 10$) of $5.42 \mu\text{g L}^{-1}$. The repeatability of the developed method was further investigated via determination of $50 \mu\text{g L}^{-1}$ UO_2^{2+} at varied intervals. The intraday ($n = 5$) and interday ($n = 5$) relative standard deviation (RSD) were calculated to be 3.33 % and 6.23 %, respectively, evidencing the high repeatability. Although our proposed MSPE-VU-vis method based on $\text{TpDb-AO@Fe}_3\text{O}_4$ gave comparable LOD, compared with other reported methods for the detection of UO_2^{2+} , the utilization of magnetic separation makes the extraction in our work more convenient than the other methods involving column or dispersive solid-phase extraction (Table 1), highlighting the advantages and potential of the proposed method for practical applications.

Table 1

Comparison of the proposed method with other reported spectral analysis methods.

Adsorbent	LOD ($\mu\text{g L}^{-1}$)	Linear ranges ($\mu\text{g L}^{-1}$)	Detection	References
ions imprinted polymer	2.55	8.51–500	Column-SPE-ID	[33]
multiwalled carbon nanotube	0.5	2.5–100	DSPE-ICP-MS	[34]
zirconium-based MOF	0.9	0–1000	DSPE-UV-vis	[35]
murexide-functionalized magnetic nanoparticles	1	20–400	MSPE-UV-vis	[36]
functionalized SBA-15	10	33.5–500	SPE-UV-vis	[37]
Fe-Al-Mn nanocomposite	9.7	/	SPE-UV-vis	[38]
magnetic graphene oxide	0.9	5–2000	MSPE-UV-vis	[17]
salen-functionalized spherical agarose-coated magnetic nanoparticles	10	30–15,000	MSPE-UV-vis	[39]
mixed-ligands resin	238	4760–119,000	SPE-UV-vis	[40]
$\text{TpDb-AO@Fe}_3\text{O}_4$	1.63	10–200	MSPE-UV-vis	present method

3.6. Real sample analysis

The discharge of nuclear wastewater into marine ecosystems significantly heightens concerns regarding uranium contamination in seafood. Thus, the developed $\text{TpDb-AO@Fe}_3\text{O}_4$ based MSPE-UV-vis was applied to analyze some seafood samples including tuna, eel, hairtail, yesso scallop and kelp. The matrix effect (ME) of these real samples after extraction was calculated to be 3.39 %–8.47 % (Table S2 and Fig. S17), indicating the effective removal of matrix interferences [41]. Notably, UO_2^{2+} was detected exclusively in hairtail samples at a concentration of $16.9 \pm 0.6 \mu\text{g kg}^{-1}$ ($16.8941 \mu\text{g kg}^{-1}$ with ICP-MS), whereas no detectable levels were found in the tuna, eel, yesso scallop and kelp samples (Table 2). Various concentrations of UO_2^{2+} (10, 50, and $100 \mu\text{g kg}^{-1}$) were further spiked into these real samples. The spiked recoveries were calculated in the range of 94.1 % – 106.8 %. This outstanding level of accuracy underscores the efficacy and precision of our approach in quantifying uranium contaminants within seafood matrices, thereby contributing to enhanced food safety surveillance. The spiked and un-spiked hairtail samples gave evident UV-vis adsorption spectrums, further illustrating the great selectivity and enrichment of $\text{TpDb-AO@Fe}_3\text{O}_4$ for UO_2^{2+} (Fig. S18).

4. Conclusion

In summary, we have successfully synthesized a magnetic amidoxime COF via an amorphous-to-crystalline method as adsorbent, and further developed its MSPE coupled with UV-vis method for detection of the UO_2^{2+} in seafood samples. The amidoxime offers the COF selective adsorption ability to UO_2^{2+} . The introduced magnetic characteristic makes sure the amidoxime COF easy to be separated from solution under the external magnetic field. Consequently, the magnetic amidoxime COF can serve as excellent adsorbent for MSPE of UO_2^{2+} . To couple with UV-vis method, our novel analytical methodology demonstrates exceptional simplicity, precision, and versatility in analyzing UO_2^{2+} in various seafood samples with low LOD, broad linear range, and great reproducibility. This approach represents an advancement in the rapid extraction and sensitive quantification of trace uranium contaminants in food matrices, thereby contributing to enhanced environmental monitoring and public health safeguards.

Table 2

Analytical result of UO_2^{2+} in real samples ($n = 3$).

Sample	Spiked ($\mu\text{g kg}^{-1}$)	Detected ($\mu\text{g kg}^{-1}$, mean \pm s)	Recovery (% , mean \pm s)
tuna	0	ND ^a	/
	10	9.7 ± 0.8	96.9 ± 8.5
	50	48.7 ± 0.9	97.3 ± 1.8
	100	106.2 ± 1.7	106.2 ± 1.7
eel	0	ND ^a	/
	10	10.3 ± 0.6	102.6 ± 5.5
	50	48.1 ± 1.7	96.2 ± 3.4
	100	95.7 ± 2.2	95.7 ± 2.2
hairtail	0	16.9 ± 0.6	/
	10	27.5 ± 1.0	105.9 ± 4.0
	50	70.3 ± 2.5	106.8 ± 3.8
	100	117.6 ± 4.3	100.7 ± 3.7
yesso scallop	0	ND ^a	/
	10	9.4 ± 0.4	94.1 ± 3.9
	50	50.2 ± 2.1	100.5 ± 4.2
	100	102.3 ± 2.4	102.3 ± 2.4
kelp	0	ND ^a	/
	10	10.4 ± 0.5	104.0 ± 4.7
	50	51.4 ± 1.6	102.7 ± 3.3
	100	102.1 ± 2.9	102.1 ± 2.9

^a ND indicates that UO_2^{2+} is not determined in the sample.

CRedit authorship contribution statement

Fan Bai: Writing – original draft, Methodology, Data curation. **Xu Yang:** Writing – review & editing. **Cheng Yang:** Methodology. **Hai-Long Qian:** Writing – review & editing, Supervision, Conceptualization. **Xiu-Ping Yan:** Writing – review & editing, Funding acquisition.

Declaration of competing interest

The authors declare that they have no known competing financial interests or personal relationships that could have appeared to influence the work reported in this paper.

Acknowledgments

This work was supported by the National Natural Science Foundation of China (22076066, 22376082 and 22422406), and the “Fundamental Research Funds for the Central Universities”.

Supplementary materials

Supplementary material associated with this article can be found, in the online version, at [doi:10.1016/j.chroma.2024.465564](https://doi.org/10.1016/j.chroma.2024.465564).

Data availability

Data will be made available on request.

References

- A.M. Macfarlane, M. Miller, Nuclear energy and uranium resources, *Elements* 3 (2007) 185–192.
- N. Kamei-Ishikawa, A. Ito, K. Tagami, T. Umita, Fate of radiocesium in sewage treatment process released by the nuclear accident at Fukushima, *Chemosphere* 93 (4) (2013) 689–694.
- Z. Li, R. Chen, T. Zhou, C. Liu, Z. Wang, G. Si, Q. Xue, Research on calculation and verification of hazardous area for radioactive sewage entering into the ocean, *Prog. Nucl. Energy* 161 (2023) 104739.
- L.D. Kraemer, D. Evans, Uranium bioaccumulation in a freshwater ecosystem: impact of feeding ecology, *Aquat. Toxicol.* 124–125 (2012) 163–170.
- A. Günther, G. Bernhard, G. Geipel, T. Reich, A. Roßberg, H. Nitsche, Uranium speciation in plants, *Radiochim. Acta* 91 (6) (2003) 319–328.
- W. Liu, X. Dai, Z. Bai, Y. Wang, Z. Yang, L. Zhang, L. Xu, L. Chen, Y. Li, D. Gui, et al., Highly sensitive and selective uranium detection in natural water systems using a luminescent mesoporous metal-organic framework equipped with abundant lewis basic sites: a combined batch, X-ray absorption spectroscopy, and first principles simulation investigation, *Environ. Sci. Technol.* 51 (7) (2017) 3911–3921.
- K.L. Cooper, E.J. Dashner, R. Tsosie, Y.M. Cho, J. Lewis, L.G. Hudson, Inhibition of poly(ADP-ribose)polymerase-1 and DNA repair by uranium, *Toxicol. Appl. Pharmacol.* 291 (2016) 13–20.
- Y.C. Yue, M.H. Li, H.B. Wang, B.L. Zhang, W. He, The toxicological mechanisms and detoxification of depleted uranium exposure, *Environ. Health Prev. Med.* 23 (1) (2018) 18.
- M.A. McDiarmid, J.P. Keogh, F.J. Hooper, K. McPhaul, K. Squibb, R. Kane, R. DiPino, M. Kabat, B. Kaup, L. Anderson, Health effects of depleted uranium on exposed Gulf War veterans, *Environ. Res.* 82 (2) (2000) 168–180.
- C. Wang, Y. Pei, P. Liu, Y. Li, Z. Wang, Donor-acceptor structure-dependent electrochemiluminescence sensor for accurate uranium detection in drinking water, *ACS Sustainable Chem. Eng.* 10 (45) (2022) 14665–14670.
- H.L. Jiang, Q.B. Fu, M.L. Wang, J.M. Lin, R.S. Zhao, Determination of trace bisphenols in functional beverages through the magnetic solid-phase extraction with MOF-COF composite, *Food Chem.* 345 (2021) 128841.
- C. McCullum, P. Tchounwou, L.-S. Ding, X. Liao, Y.-M. Liu, Extraction of aflatoxins from liquid foodstuff samples with polydopamine-coated superparamagnetic nanoparticles for HPLC-MS/MS Analysis, *J. Agric. Food Chem.* 62 (19) (2014) 4261–4267.
- F. Wei, Q. Zhao, X. Lv, X.-Y. Dong, Y.-Q. Feng, H. Chen, Rapid magnetic solid-phase extraction based on monodisperse magnetic single-crystal ferrite nanoparticles for the determination of free fatty acid content in edible oils, *J. Agric. Food Chem.* 61 (1) (2013) 76–83.
- G.-R. Li, M.-Y. Xu, J.-K. Li, Y. Yang, A study on the preparation and application of a core-shell surface imprinted uranyl magnetic chelating adsorbent, *RSC Adv.* 8 (65) (2018) 37401–37409.
- L.-Q. He, Z.-M. Wang, Y.-J. Li, J. Yang, L.-F. Liao, X.-L. Xiao, Y. Liu, A novel electrochemical sensor modified with a computer-simulative magnetic ion-imprinted membrane for identification of uranyl ion, *Sensors* 22 (12) (2022) 4410.
- E. Zolfonoun, S.R. Yousefi, Sorption and preconcentration of uranium and thorium from aqueous solutions using multi-walled carbon nanotubes decorated with magnetic nanoparticles, *Radiochim. Acta* 103 (12) (2015) 835–841.
- A. Amini, M. Khajeh, A.R. Oveisi, S. Daliran, M. Ghaffari-Moghaddam, H. S. Delarami, A porous multifunctional and magnetic layered graphene oxide/3D mesoporous MOF nanocomposite for rapid adsorption of uranium(VI) from aqueous solutions, *J. Ind. Eng. Chem.* 93 (2021) 322–332.
- X. Zhang, L. Chen, L. Fu, K. Feng, J. Gong, J. Qu, R. Niu, Dual-functional metal-organic frameworks-based hydrogel micromotor for uranium detection and removal, *J. Hazard. Mater.* 467 (2024) 133654.
- J.-C. Yin, Y.-S. Wang, B. Zhou, X.-L. Xiao, J.-H. Xue, J.-C. Wang, Y.-S. Wang, Q.-M. Qian, A wireless magnetoelastic sensor for uranyl using DNzyme-graphene oxide and gold nanoparticles-based amplification, *Sens. Actuators B* 188 (2013) 147–155.
- W.R. Cui, C.R. Zhang, W. Jiang, F.F. Li, R.P. Liang, J. Liu, J.D. Qiu, Regenerable and stable sp² carbon-conjugated covalent organic frameworks for selective detection and extraction of uranium, *Nat. Commun.* 11 (1) (2020) 436.
- W. He, Z. Qiu, Q. Sun, Z. Li, Z. Chen, L. Hu, H. Wang, Amidoxime-functionalized hollow 2D-COFs for uranium separation, *Sep. Purif. Technol.* 331 (2024) 125620.
- C.-R. Zhang, W.-R. Cui, W. Jiang, F.-F. Li, Y.-D. Wu, R.-P. Liang, J.-D. Qiu, Simultaneous sensitive detection and rapid adsorption of UO₂²⁺ based on a post-modified sp² carbon-conjugated covalent organic framework, *Environ. Sci.* 7 (3) (2020) 842–850.
- F.-F. Li, W.-R. Cui, W. Jiang, C.-R. Zhang, R.-P. Liang, J.-D. Qiu, Stable sp² carbon-conjugated covalent organic framework for detection and efficient adsorption of uranium from radioactive wastewater, *J. Hazard. Mater.* 392 (2020) 122333.
- Y. Xie, Y. Wu, X. Liu, M. Hao, Z. Chen, G.I.N. Waterhouse, X. Wang, H. Yang, S. Ma, Rational design of cooperative chelating sites on covalent organic frameworks for highly selective uranium extraction from seawater, *Cell Rep. Phys. Sci.* 4 (1) (2023) 101220.
- G. Cheng, A. Zhang, Z. Zhao, Z. Chai, B. Hu, B. Han, Y. Ai, X. Wang, Extremely stable amidoxime functionalized covalent organic frameworks for uranium extraction from seawater with high efficiency and selectivity, *Sci. Bull. (Beijing)* 66 (19) (2021) 1994–2001.
- B. Yan, C. Ma, J. Gao, Y. Yuan, N. Wang, An ion-crosslinked supramolecular hydrogel for ultrahigh and fast uranium recovery from seawater, *Adv. Mater.* 32 (10) (2020) 1906615.
- D.G. Li, Y.Z. Liao, Z. Chen, X.X. Chang, X. Zhang, C.C. Chen, C. Cui, Z.L. Zhang, C. Muhire, W.W. Tang, A 3D hierarchical porous adsorbent constructed by cryopolymerization for ultrafast uranium harvesting from seawater, *J. Mater. Chem. A* 11 (19) (2023) 10384–10395.
- J. Tan, S. Namuangruk, W. Kong, N. Kungwan, J. Guo, C. Wang, Manipulation of amorphous-to-crystalline transformation: towards the construction of covalent organic framework hybrid microspheres with NIR photothermal conversion ability, *Angew. Chem. Int. Ed. Engl.* 55 (45) (2016) 13979–13984.
- Y. Li, C.X. Yang, X.P. Yan, Controllable preparation of core-shell magnetic covalent-organic framework nanospheres for efficient adsorption and removal of bisphenols in aqueous solution, *Chem. Commun. (Camb.)* 53 (16) (2017) 2511–2514.
- M.H. Khan, P. Warwick, N. Evans, Spectrophotometric determination of uranium with arsenazo-III in perchloric acid, *Chemosphere* 63 (7) (2006) 1165–1169.
- M.J. Manos, M.G. Kanatzidis, Layered metal sulfides capture uranium from seawater, *J. Am. Chem. Soc.* 134 (39) (2012) 16441–16446.
- M.J. Kang, B.E. Han, P.S. Hahn, Precipitation and adsorption of uranium(VI) under various aqueous conditions, *Environ. Eng. Res.* 7 (3) (2002) 149–157.
- C.S.A. Felix, A.V.B. Chagas, R.F. de Jesus, W.T. Barbosa, J.D.V. Barbosa, S.L.C. Ferreira, V. Cerdá, Synthesis and application of a new polymer with imprinted ions for the preconcentration of uranium in natural water samples and determination by digital imaging, *28(10)* (2023), 4065.
- F. Aydin, E. Yilmaz, E. Ölmez, M. Soylak, Cu₂O-CuO ball like/multiwalled carbon nanotube hybrid for fast and effective ultrasound-assisted solid phase extraction of uranium at ultra-trace level prior to ICP-MS detection, *Talanta* 207 (2020) 120295.
- M. Sharifi-Rad, M. Kaykhai, M. Khajeh, A. Oveisi, Synthesis, characterization and application of a zirconium-based MOF-808 functionalized with isonicotinic acid for fast and efficient solid phase extraction of uranium(VI) from wastewater prior to its spectrophotometric determination, *BMC Chem.* 16 (1) (2022) 27.
- T. Oymak, Solid-phase extraction method by magnetic nanoparticles functionalized with murexide for trace U(VI) from sea water prior to spectrophotometric determination, *Acta Chim. Slov.* (2019) 78–84.
- L. Dolatyari, M.R. Yaftian, S. Rostamnia, M.S. Seyeddorraj, Multivariate optimization of a functionalized SBA-15 mesoporous based solid-phase extraction for U(VI) determination in water samples, *Anal. Sci.* 33 (7) (2017) 769–776.
- A.M. Dinkir, A.M. Tadesse, T. Kebede, Chelating agent-free solid phase extraction (CAF-SPE) of uranium, cadmium and lead by Fe-Al-Mn nanocomposite from aqueous solution, *J. Mater. Sci.* 33 (26) (2022) 21034–21047.
- F. Nazari Serenjah, P. Hashemi, H. Naeimi, E. Zakerzadeh, A.R. Ghiasvand, Spherical agarose-coated magnetic nanoparticles functionalized with a new salen for magnetic solid-phase extraction of uranyl ion, *Microchim. Acta* 183 (8) (2016) 2449–2455.
- M.S. Hosseini, F. Abedi, Stepwise extraction of Th(IV) and U(VI) ions with mixed-ligands impregnated resin containing 1,4-diaminoanthraquinone and 1,4-dihydroxyanthraquinone, *J. Radioanal. Nucl. Chem.* 303 (1) (2015) 209–216.
- L.-H. Su, H.-L. Qian, C. Yang, C. Wang, Z. Wang, X.-P. Yan, Integrating molecular imprinting into flexible covalent organic frameworks for selective recognition and efficient extraction of aflatoxins, *J. Hazard. Mater.* 467 (2024) 133755.